

Reduction of large-scale RLCK models via low-rank balanced truncation

Christos Giamouzis, Dimitrios Garyfallou, Anastasis Vagenas,
and Nestor Evmorfopoulos

Dept. of Electrical and Computer Engineering, University of Thessaly, Volos, Greece
{cgiamouzis, digaryfa, avagenas, nestevmo}@e-ce.uth.gr

Abstract

Model order reduction (MOR) is an important step in the design process of integrated circuits. Specifically, the electromagnetic models extracted from modern complex designs result in a large number of passive elements that introduce limitations in the simulation process. MOR techniques based on balanced truncation (BT) can overcome these limitations by producing compact reduced-order models (ROMs) that approximate the behavior of the original models at the input/output ports. In this paper, we present a low-rank BT method that exploits the extended Krylov subspace and efficient implementation techniques for the reduction of large-scale models. Experimental evaluation on a diverse set of analog and mixed-signal circuits with millions of elements indicates that up to $\times 5.5$ smaller ROMs can be produced with similar accuracy to ANSYS RaptorX™ ROMs.

1 Introduction

Electromagnetic model extraction plays a key role in the design and analysis of integrated circuits. The extracted models are simulated to accurately predict the behavior of the passive elements of the design. Model order reduction (MOR) can reduce the complexity of RLCK models with many elements ($>1M$) and ports (>10), while retaining an accurate approximation of the input and output behavior of the circuit [1, 2]. Therefore, the simulation time of complex systems can be radically decreased by constructing reduced-order models (ROMs) of smaller dimensions that preserve the essential characteristics of the original models.

MOR methods are distinguished into two main categories. Moment matching (MM) techniques [1] are preferred due to their computational efficiency. However, they rely on an ad hoc selection of the number of moments, which correlates the final ROM size with the number of ports. On the other hand, techniques based on balanced truncation (BT) [2] offer reliable bounds for the approximation error and have no fundamental limitation to the number of ports they can handle, resulting in more compact ROMs. Nevertheless, BT applies only to small-scale models since it involves the computationally expensive solution of Lyapunov equations [2].

In this work, appropriate performance improvements are explored to overcome the main drawback of the conventional BT method. To this end, we adopt an efficient low-rank technique based on the extended Krylov subspace (EKS) for solving the Lyapunov equations. The proposed approach can be integrated into industrial extraction tools, such as the ANSYS RaptorX™ [3], to obtain more compact ROMs of large-scale multi-port RLCK models.

2 Background

Consider the modified nodal analysis (MNA) description [4] of an n -node, m -branch (inductive), p -input, and q -output RLCK circuit in the time domain:

$$\begin{pmatrix} \mathbf{G}_n & \mathbf{E} \\ -\mathbf{E}^T & \mathbf{0} \end{pmatrix} \begin{pmatrix} \mathbf{v}(t) \\ \mathbf{i}(t) \end{pmatrix} + \begin{pmatrix} \mathbf{C}_n & \mathbf{0} \\ \mathbf{0} & \mathbf{M} \end{pmatrix} \begin{pmatrix} \dot{\mathbf{v}}(t) \\ \dot{\mathbf{i}}(t) \end{pmatrix} = \begin{pmatrix} \mathbf{B}_1 \\ \mathbf{0} \end{pmatrix} \mathbf{u}(t), \quad \mathbf{y}(t) = \begin{pmatrix} \mathbf{L}_1 & \mathbf{0} \end{pmatrix} \begin{pmatrix} \mathbf{v}(t) \\ \mathbf{i}(t) \end{pmatrix} \quad (1)$$

where $\mathbf{G}_n \in \mathbb{R}^{n \times n}$ (node conductance matrix), $\mathbf{C}_n \in \mathbb{R}^{n \times n}$ (node capacitance matrix), $\mathbf{M} \in \mathbb{R}^{m \times m}$ (branch inductance matrix), $\mathbf{E} \in \mathbb{R}^{n \times m}$ (node-to-branch incidence matrix), $\mathbf{v} \in \mathbb{R}^n$ (vector of node voltages), $\mathbf{i} \in \mathbb{R}^m$ (vector of inductive branch currents), $\mathbf{u} \in \mathbb{R}^p$ (vector of input excitations), $\mathbf{B}_1 \in \mathbb{R}^{n \times p}$ (input-to-node connectivity matrix), $\mathbf{y} \in \mathbb{R}^q$ (vector of output measurements), and $\mathbf{L}_1 \in \mathbb{R}^{q \times n}$ (node-to-output connectivity matrix). Moreover, we denote $\dot{\mathbf{v}}(t) \equiv \frac{d\mathbf{v}(t)}{dt}$ and $\dot{\mathbf{i}}(t) \equiv \frac{d\mathbf{i}(t)}{dt}$. If we now define the model order as $N \equiv n + m$, the state vector as $\mathbf{x}(t) \equiv \begin{pmatrix} \mathbf{v}(t) \\ \mathbf{i}(t) \end{pmatrix}$, and also:

$$\mathbf{G} \equiv - \begin{pmatrix} \mathbf{G}_n & \mathbf{E} \\ -\mathbf{E}^T & \mathbf{0} \end{pmatrix}, \quad \mathbf{C} \equiv \begin{pmatrix} \mathbf{C}_n & \mathbf{0} \\ \mathbf{0} & \mathbf{M} \end{pmatrix}, \quad \mathbf{B} \equiv \begin{pmatrix} \mathbf{B}_1 \\ \mathbf{0} \end{pmatrix}, \quad \mathbf{L} \equiv (\mathbf{L}_1 \quad \mathbf{0}),$$

then Eq. (1) can be written in the generalized state-space form, or so-called descriptor form:

$$\mathbf{C} \frac{d\mathbf{x}(t)}{dt} = \mathbf{G}\mathbf{x}(t) + \mathbf{B}\mathbf{u}(t), \quad \mathbf{y}(t) = \mathbf{L}\mathbf{x}(t). \quad (2)$$

The objective of MOR is to produce an equivalent ROM:

$$\tilde{\mathbf{C}} \frac{d\tilde{\mathbf{x}}(t)}{dt} = \tilde{\mathbf{G}}\tilde{\mathbf{x}}(t) + \tilde{\mathbf{B}}\mathbf{u}(t), \quad \tilde{\mathbf{y}}(t) = \tilde{\mathbf{L}}\tilde{\mathbf{x}}(t) \quad (3)$$

where $\tilde{\mathbf{G}}, \tilde{\mathbf{C}} \in \mathbb{R}^{r \times r}$, $\tilde{\mathbf{B}} \in \mathbb{R}^{r \times p}$, $\tilde{\mathbf{L}} \in \mathbb{R}^{q \times r}$, the reduced order $r \ll N$, and the output error is bounded as $\|\tilde{\mathbf{y}}(t) - \mathbf{y}(t)\|_2 < \varepsilon \|\mathbf{u}(t)\|_2$ for given $\mathbf{u}(t)$ and small ε . The output error bound can be expressed in the frequency domain as $\|\tilde{\mathbf{y}}(s) - \mathbf{y}(s)\|_2 < \varepsilon \|\mathbf{u}(s)\|_2$ via Plancherel's theorem [5]. If

$$\mathbf{H}(s) = \mathbf{L}(s\mathbf{C} - \mathbf{G})^{-1}\mathbf{B}, \quad \tilde{\mathbf{H}}(s) = \tilde{\mathbf{L}}(s\tilde{\mathbf{C}} - \tilde{\mathbf{G}})^{-1}\tilde{\mathbf{B}}$$

are the transfer functions of the original model and the ROM, the corresponding output error is:

$$\|\tilde{\mathbf{y}}(s) - \mathbf{y}(s)\|_2 = \|\tilde{\mathbf{H}}(s)\mathbf{u}(s) - \mathbf{H}(s)\mathbf{u}(s)\|_2 \leq \|\tilde{\mathbf{H}}(s) - \mathbf{H}(s)\|_\infty \|\mathbf{u}(s)\|_2 \quad (4)$$

where $\|\cdot\|_\infty$ is the \mathcal{L}_2 matrix norm or \mathcal{H}_∞ norm of a rational transfer function. Thus, to bound this error, we need to bound the distance between the transfer functions: $\|\tilde{\mathbf{H}}(s) - \mathbf{H}(s)\|_\infty < \varepsilon$.

3 MOR by Balanced Truncation

BT relies on the computation of the controllability Gramian \mathbf{P} and observability Gramian \mathbf{Q} , which are calculated as the solutions of the following Lyapunov matrix equations [2]:

$$(\mathbf{C}^{-1}\mathbf{G})\mathbf{P} + \mathbf{P}(\mathbf{C}^{-1}\mathbf{G})^T = -(\mathbf{C}^{-1}\mathbf{B})(\mathbf{C}^{-1}\mathbf{B})^T, \quad (\mathbf{C}^{-1}\mathbf{G})^T\mathbf{Q} + \mathbf{Q}(\mathbf{C}^{-1}\mathbf{G}) = -\mathbf{L}^T\mathbf{L}. \quad (5)$$

The controllability Gramian \mathbf{P} characterizes the input-to-state behavior, i.e., the degree to which the states are controllable by the inputs, while the observability Gramian \mathbf{Q} characterizes the state-to-output behavior, i.e., the degree to which the states are observable at the outputs. In principle, a ROM can be obtained by eliminating the states that are difficult to reach or observe. However, in the original state-space coordinates, there are states that are difficult to reach but easy to observe, and vice versa. The process of ‘‘balancing’’ transforms the state vector to a new coordinate system, where for each state, the degree of difficulty is the same for both reaching and observing it. An appropriate transformation $\mathbf{T}\mathbf{x}(t)$ exists, leading to the following model:

$$\mathbf{T}\mathbf{C}\mathbf{T}^{-1} \frac{d(\mathbf{T}\mathbf{x}(t))}{dt} = \mathbf{T}\mathbf{G}\mathbf{T}^{-1}(\mathbf{T}\mathbf{x}(t)) + \mathbf{T}\mathbf{B}\mathbf{u}(t), \quad \mathbf{y}(t) = \mathbf{L}\mathbf{T}^{-1}(\mathbf{T}\mathbf{x}(t)) \quad (6)$$

that preserves the transfer function $\mathbf{H}(s)$. This renders $\mathbf{P} = \mathbf{Q} = \text{diag}(\sigma_1, \sigma_2, \dots, \sigma_N)$ [2], where σ_i are known as the Hankel singular values (HSVs) of the model and are equal to the square roots of the eigenvalues of product $\mathbf{P}\mathbf{Q}$, i.e., $\sigma_i = \sqrt{\lambda_i(\mathbf{P}\mathbf{Q})}$. In the above balanced model, the states that are easier to reach and observe correspond to the largest HSVs. If r of them are preserved (truncating the $N - r$ states corresponding to the smallest HSVs), it can be shown that the distance between the original and the reduced-order transfer functions is bounded as:

$$\|\mathbf{H}(s) - \tilde{\mathbf{H}}(s)\|_\infty \leq 2(\sigma_{r+1} + \sigma_{r+2} + \dots + \sigma_N) \quad (7)$$

The latter is an ‘‘a-priori’’ criterion for selecting the ROM order for a desired output error tolerance ε , which constitutes a significant advantage of BT over MM techniques. The main steps of the BT procedure are summarized in Algorithm 1. The major drawback of BT is the significant

Algorithm 1 MOR by balanced truncation

- 1: Solve the Lyapunov equations to obtain the Gramian matrices \mathbf{P} and \mathbf{Q} [6]
 - 2: Compute the SVD of the Gramian matrices: $\mathbf{P} = \mathbf{U}_P \boldsymbol{\Sigma}_P \mathbf{V}_P^T$ and $\mathbf{Q} = \mathbf{U}_Q \boldsymbol{\Sigma}_Q \mathbf{V}_Q^T$
 - 3: Find the square root of the Gramian matrices: $\mathbf{Z}_P = \mathbf{U}_P \boldsymbol{\Sigma}_P^{1/2}$ and $\mathbf{Z}_Q = \mathbf{U}_Q \boldsymbol{\Sigma}_Q^{1/2}$
 - 4: Compute the SVD of the product of the roots: $\mathbf{Z}_Q^T \mathbf{Z}_P = \mathbf{U} \boldsymbol{\Sigma} \mathbf{V}^T$
 - 5: Compute transformation matrices: $\mathbf{T}_{(r \times N)} = \boldsymbol{\Sigma}_{(r \times r)}^{-1/2} \mathbf{U}_{(r \times N)} \mathbf{Z}_Q^T$, $\mathbf{T}_{(N \times r)}^{-1} = \mathbf{Z}_P \mathbf{V}_{(N \times r)} \boldsymbol{\Sigma}_{(r \times r)}^{-1/2}$
 - 6: Compute ROM: $\tilde{\mathbf{G}} = \mathbf{T}_{(r \times N)} \mathbf{G} \mathbf{T}_{(N \times r)}^{-1}$, $\tilde{\mathbf{C}} = \mathbf{T}_{(r \times N)} \mathbf{C} \mathbf{T}_{(N \times r)}^{-1}$, $\tilde{\mathbf{B}} = \mathbf{T}_{(r \times N)} \mathbf{B}$, $\tilde{\mathbf{L}} = \mathbf{L} \mathbf{T}_{(N \times r)}^{-1}$
-

computational and memory cost for deriving the ROM, which hinders the applicability to large-scale models (with N over a few thousand states). This is because the operations involved (e.g., the solution of Lyapunov equations and the singular value decomposition [SVD]) are computationally expensive with a complexity of $O(N^3)$. Moreover, they are applied on dense matrices, since the Gramians \mathbf{P}, \mathbf{Q} are dense even if the system matrices $\mathbf{C}, \mathbf{G}, \mathbf{B}, \mathbf{L}$ are sparse.

However, the products $(\mathbf{C}^{-1} \mathbf{B})(\mathbf{C}^{-1} \mathbf{B})^T$ and $\mathbf{L}^T \mathbf{L}$ have low numerical order compared to N , as $p, q \ll N$, resulting in low-rank Gramian matrices that can be approximated using low-rank techniques. This greatly reduces the complexity and memory requirements of the solution of the Lyapunov equations and the SVD analysis, which are now of order k instead of full order N .

3.1 Low-rank BT MOR

The essence of low-rank BT MOR is to iteratively project the Lyapunov equations of Eq. (5) onto a lower-dimensional Krylov subspace and then solve the resulting small-scale equations to obtain low-rank approximate solutions of Eq. (5). More specifically, if $\mathbf{K} \in \mathbb{R}^{N \times k}$ ($k \ll N$) is a projection matrix whose columns span the k -dimensional Krylov subspace:

$$\mathcal{K}_k(\mathbf{G}_C, \mathbf{B}_C) = \text{span}\{\mathbf{B}_C, \mathbf{G}_C \mathbf{B}_C, \mathbf{G}_C^2 \mathbf{B}_C, \dots, \mathbf{G}_C^{k-1} \mathbf{B}_C\}$$

where $\mathbf{G}_C \equiv \mathbf{C}^{-1} \mathbf{G}$, $\mathbf{B}_C \equiv \mathbf{C}^{-1} \mathbf{B}$, then the projected Lyapunov equation (for the controllability Gramian \mathbf{P}) onto $\mathcal{K}_k(\mathbf{G}_C, \mathbf{B}_C)$ is:

$$(\mathbf{K}^T \mathbf{G}_C \mathbf{K}) \mathbf{X} + \mathbf{X} (\mathbf{K}^T \mathbf{G}_C \mathbf{K})^T = -\mathbf{K}^T \mathbf{B}_C \mathbf{B}_C^T \mathbf{K} \quad (8)$$

(the same holds true for the observability Gramian \mathbf{Q} with $\mathbf{G}_C^T, \mathbf{L}^T$ in place of $\mathbf{G}_C, \mathbf{B}_C$). The solution $\mathbf{X} \in \mathbb{R}^{k \times k}$ of Eq. (8) can be back-projected to the N -dimensional space to give an approximate solution $\mathbf{P} = \mathbf{K} \mathbf{X} \mathbf{K}^T$ for the original large-scale Eq. (5), and a low-rank factor $\mathbf{Z} \in \mathbb{R}^{N \times k}$ of \mathbf{P} can be obtained as $\mathbf{Z} = \mathbf{K} \mathbf{U} \boldsymbol{\Sigma}^{1/2}$, where $[\mathbf{U}, \boldsymbol{\Sigma}, \mathbf{V}] = \text{SVD}(\mathbf{X})$.

Although the projection process is independent of the subspace selection, its effectiveness is critically dependent on the chosen subspace. The convergence to the final solution can be

accelerated by enriching the standard Krylov subspace $\mathcal{K}_k(\mathbf{G}_C, \mathbf{B}_C)$ with information from the subspace $\mathcal{K}_k(\mathbf{G}_C^{-1}, \mathbf{B}_C)$, which corresponds to the inverse matrix \mathbf{G}_C^{-1} , leading to the EKS [7, 8]:

$$\mathcal{K}_k^C(\mathbf{G}_C, \mathbf{B}_C) = \text{span}\{\mathbf{B}_C, \mathbf{G}_C^{-1}\mathbf{B}_C, \mathbf{G}_C\mathbf{B}_C, \mathbf{G}_C^{-2}\mathbf{B}_C, \mathbf{G}_C^2\mathbf{B}_C, \dots, \mathbf{G}_C^{-(k-1)}\mathbf{B}_C, \mathbf{G}_C^{k-1}\mathbf{B}_C\} \quad (9)$$

The EKS method (EKSM) starts with the pair $\{\mathbf{B}_C, \mathbf{G}_C^{-1}\mathbf{B}_C\}$ and generates an extended subspace $\mathcal{K}_k^C(\mathbf{G}_C, \mathbf{B}_C)$ of increasing dimension, solving the projected Lyapunov Eq. (8) in each iteration, until a sufficiently accurate approximation of the solution of Eq. (5) is obtained. The complete EKSM is presented in Algorithm 2. Below are some efficient implementation details:

- **Matrix inversion by linear solves:** The inputs to Algorithm 2 are not actually $\mathbf{G}_C \equiv \mathbf{C}^{-1}\mathbf{G}$ or $\mathbf{G}_C^T \equiv (\mathbf{C}^{-1}\mathbf{G})^T$ but the system matrices \mathbf{G} , \mathbf{C} or \mathbf{G}^T , \mathbf{C}^T , since the (generally dense) inverse matrices are only needed in products with p vectors (in step 2) and $2pj$ vectors (in steps 4 and 11 of each iteration). These can be implemented as linear solves $\mathbf{C}\mathbf{Y} = \mathbf{R}$ and $\mathbf{G}\mathbf{Y} = \mathbf{R}$ (or $\mathbf{C}^T\mathbf{Y} = \mathbf{R}$, $\mathbf{G}^T\mathbf{Y} = \mathbf{R}$) by any direct or iterative algorithm like [9].
- **Handling of sparse/dense matrices:** Note that matrix \mathbf{M} of Eq. (1) is highly dense, as it generally includes a huge number of mutual inductances. To effectively handle the sparse (\mathbf{C}_n) and dense (\mathbf{M}) blocks of matrix \mathbf{C} , we use efficient data structures and numerical techniques. For example, for linear solves and matrix-vector products, we employ parallel CPU-optimized methods for sparse matrices and leverage GPU-accelerated techniques [10] for dense matrices.
- **Solution of the small-scale Lyapunov equations:** To solve the small-scale ($2pj \times 2pj$) Lyapunov equations in step 5 of each iteration, we employ the Bartels-Stewart algorithm [6].
- **Convergence criterion:** An appropriate stopping criterion is the residual of Eq. (5) with the approximate solution $\mathbf{P} = \mathbf{K}\mathbf{K}^T$ to reach a certain threshold in magnitude, i.e.,

$$\frac{\|\mathbf{G}_C\mathbf{K}^{(j)}\mathbf{X}\mathbf{K}^{(j)T} + \mathbf{K}^{(j)}\mathbf{X}\mathbf{K}^{(j)T}\mathbf{G}_C + \mathbf{B}_C\mathbf{B}_C^T\|}{\|\mathbf{B}_C\mathbf{B}_C^T\|} \leq \text{tol} \quad (10)$$

However, this criterion equals to $\|\mathbf{R}^T\mathbf{M}\mathbf{X}\| \leq \text{tol}$ [11], which can be computed more efficiently. A tolerance of $\text{tol} = 10^{-10}$ is typically adequate to obtain an accurate model.

Algorithm 2 Extended Krylov subspace method for low-rank solution of Lyapunov equations

Input: $\mathbf{G}_C \equiv \mathbf{C}^{-1}\mathbf{G}$, $\mathbf{B}_C \equiv \mathbf{C}^{-1}\mathbf{B}$ (or \mathbf{G}_C^T , \mathbf{L}^T)

Output: \mathbf{Z} such that $\mathbf{P} \approx \mathbf{Z}\mathbf{Z}^T$

- 1: $j = 1$; $p = \text{size_col}(\mathbf{B}_C)$
 - 2: $\mathbf{K}^{(j)} = \text{Orth}([\mathbf{B}_C, \mathbf{G}_C^{-1}\mathbf{B}_C])$
 - 3: **while** $j < \text{maxiter}$ **do**
 - 4: $\mathbf{A} = \mathbf{K}^{(j)T}\mathbf{G}_C\mathbf{K}^{(j)}$; $\mathbf{R} = \mathbf{K}^{(j)T}\mathbf{B}_C$
 - 5: Solve $\mathbf{A}\mathbf{X} + \mathbf{X}\mathbf{A}^T = -\mathbf{R}\mathbf{R}^T$ for $\mathbf{X} \in \mathbb{R}^{2pj \times 2pj}$
 - 6: **if** converged **then**
 - 7: $[\mathbf{U}, \mathbf{\Sigma}, \mathbf{V}] = \text{SVD}(\mathbf{X})$; $\mathbf{Z} = \mathbf{K}^{(j)}\mathbf{U}\mathbf{\Sigma}^{1/2}$
 - 8: **break**
 - 9: **end if**
 - 10: $k_1 = 2p(j-1)$; $k_2 = k_1 + p$; $k_3 = 2pj$
 - 11: $\mathbf{K}_1 = [\mathbf{G}_C\mathbf{K}^{(j)}(:, k_1+1:k_2), \mathbf{G}_C^{-1}\mathbf{K}^{(j)}(:, k_2+1:k_3)]$
 - 12: $\mathbf{K}_2 = \text{Orth}(\mathbf{K}_1)$ w.r.t. $\mathbf{K}^{(j)}$
 - 13: $\mathbf{K}_3 = \text{Orth}(\mathbf{K}_2)$
 - 14: $\mathbf{K}^{(j+1)} = [\mathbf{K}^{(j)}, \mathbf{K}_3]$
 - 15: $j = j + 1$
 - 16: **end while**
-

4 Experimental Evaluation

4.1 Experimental setup

To evaluate EKSM, we used large-scale RLCK models extracted from different circuits using ANSYS RaptorX™ [3]. These circuits consist of many passive elements, including mutual inducances. The EKSM ROMs are compared against golden ROMs produced by RaptorX™, through S-parameter plotting. The characteristics of the RLCK models are listed in Table 1. All experiments were executed on a Linux server with a 2.80 GHz 16-thread CPU and 64 GB of memory.

Table 1: Detailed characteristics of RLCK models

Model	Initial order	#nodes	#ports	#resistors	#capacitors	#inductors	#mutual ind.
VGA_28	95189	57675	13	155879	169600	37514	126766838
Hybrid_56	98024	59210	5	112338	290572	38814	165802476
Wilkinson_56	100888	60703	4	115117	271293	40185	193641938
VCO_13	104367	61264	4	604072	596846	43103	188436057
CSLNA_56	128574	78046	9	188842	472573	50528	169339965
Wilkinson_28	129087	78263	4	123254	266710	50824	259462454
Hybrid_28	134710	75766	5	128935	283905	53169	264162513
LNACASC_28	162881	96876	11	774427	684662	66005	323090671

4.2 Experimental results

The efficiency of the EKSM against RaptorX™ is demonstrated in Table 2. The S-parameter plots of Figure 1 indicate that EKSM achieves accuracy close to that of RaptorX™ while producing roughly $\times 3.1$ more compact ROMs. Although EKSM has higher reduction time and memory requirements, they are still reasonable and can be significantly improved in future work.

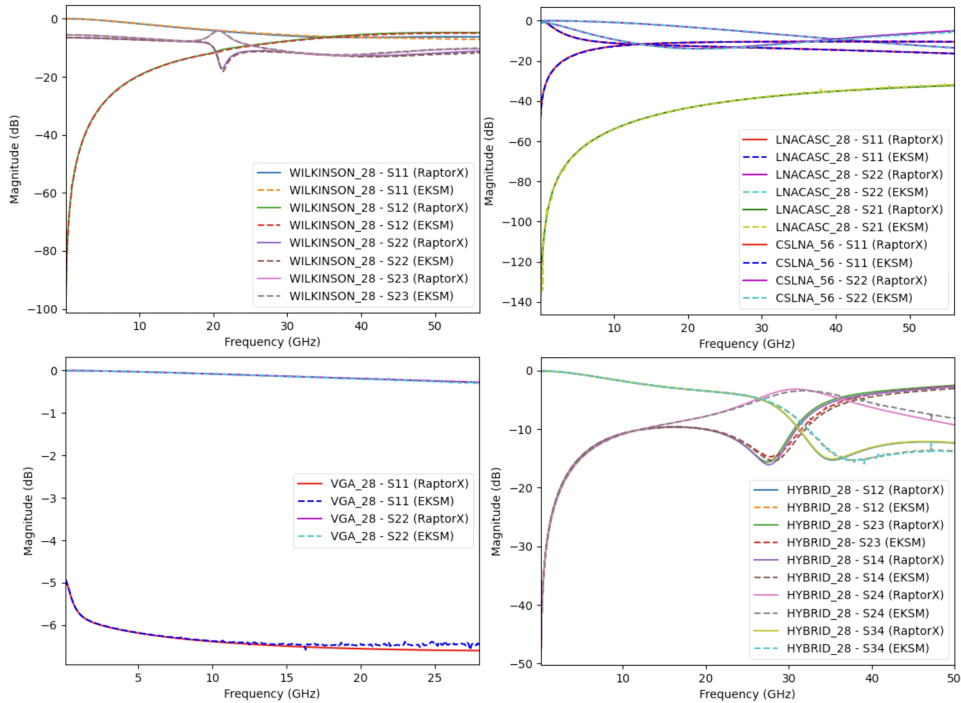


Figure 1: Comparison of accuracy between EKSM and RaptorX™ ROMs.

Table 2: ROM order and MOR performance of EKSM vs RaptorX™

Model	Initial order	ROM order		Reduction time (s)		Memory (GB)	
		RaptorX™	EKSM	RaptorX™	EKSM	RaptorX™	EKSM
VGA_28	95189	4744	1040	67	1037	32.63	19.14
Hybrid_56	98024	1267	397	104	613	24.05	29.11
Wilkinson_56	100888	765	320	154	570	24.79	29.76
VCO_13	104367	407	311	119	673	26.48	29.18
LNACS_56	128574	2172	716	74	1237	25.82	26.74
Wilkinson_28	129087	885	302	205	801	25.35	36.21
Hybrid_28	134710	787	399	217	1032	24.31	35.52
LNACasc_28	162881	4768	879	373	2866	78.52	48.67

5 Conclusions

Alternative MOR techniques to reduce large-scale RLCK models with accuracy comparable to commercial tools are presented. The proposed low-rank BT method is evaluated across diverse large-scale benchmark circuits by comparing their S-parameters. Experimental results indicate that our approach achieves sufficient accuracy while providing ROMs that are up to $\times 5.5$ smaller than the ROMs obtained by ANSYS RaptorX™.

6 Acknowledgments

This research has been co-financed by the European Regional Development Fund and Greek national funds via the Operational Program "Competitiveness, Entrepreneurship and Innovation," under the call "RESEARCH-CREATE-INNOVATE" (project code: T2EDK-00609).

References

- [1] A. Odabasioglu *et al.*, "Prima: Passive reduced-order interconnect macromodeling algorithm," *IEEE Trans. on CAD of Integrated Circuits and Systems*, vol. 17, no. 8, pp. 645–654, 1998.
- [2] S. Gugercin *et al.*, "A survey of model reduction by balanced truncation and some new results," *International Journal of Control*, vol. 77, no. 8, pp. 748–766, 2004.
- [3] "Ansys-RaptorX." [Online]. Available: www.ansys.com/products/semiconductors/ansys-raptorh
- [4] C.-W. Ho *et al.*, "The modified nodal approach to network analysis," *IEEE Trans. on Circuits and Systems*, vol. 22, no. 6, pp. 504 – 509, 1975.
- [5] K. Gröchenig, *Foundations of Time-Frequency Analysis*. Birkhäuser, 2001.
- [6] D. Lathauwer *et al.*, "Computation of the canonical decomposition by means of a simultaneous generalized schur decomposition," *SIAM Journal on Matrix Analysis and Applications*, vol. 26, no. 2, pp. 295–327, 2004.
- [7] P. Stoikos *et al.*, "The Extended and Asymmetric Extended Krylov Subspace in Moment-Matching-Based Order Reduction of Large Circuit Models," arXiv:2204.02467 [cs.OH], 2022.
- [8] C. Chatzigeorgiou *et al.*, "Exploiting Extended Krylov Subspace for the Reduction of Regular and Singular Circuit Models," in *Proc. of the 26th Asia South Pacific Design Automation Conference*, pp. 773–778, 2021.
- [9] E. Bavier *et al.*, "Amesos2 and Belos: Direct and Iterative Solvers for Large Sparse Linear Systems," *Sci. Program.*, vol. 20, no. 3, p. 241–255, jul 2012.
- [10] D. Garyfallou *et al.*, "A Combinatorial Multigrid Preconditioned Iterative Method for Large Scale Circuit Simulation on GPUs," in *Proc. of the 15th International Conference on Synthesis, Modeling, Analysis and Simulation Methods and Applications to Circuit Design*, pp. 209–212, 2018.
- [11] V. Simoncini, "A new iterative method for solving large-scale lyapunov matrix equations," *SIAM Journal on Scientific Computing*, vol. 29, no. 3, pp. 1268–1288, 2007.